SINTERING BEHAVIOR OF AN ISOLATED PORE: MONTE CARLO SIMULATION

WAN Y. SHIH, WEI-HENG SHIH, AND ILHAN A. AKSAY

Department of Materials Science and Engineering, and
Washington Technology Center, University of Washington, Seattle, WA 98195

INTRODUCTION

Microstructures play an important role in sintering. However, most existing sintering theories are macroscopic and do not consider the topological constraints in a microstructure. To fully take into account the microstructural effect, Anderson et al. [1] developed a Monte Carlo statistical mechanics model to study the grain growth behavior of a fully dense system. Here we developed a generalized model which allows both densification and grain growth to occur. The densification occurs through the diffusion of matter and is incorporated in the Monte Carlo procedure. Thus we can monitor both the microstructural evolution and the densification at the same time during heat treatment. To our knowledge, this is the first statistical mechanics model constructed for sintering. As a quantitative example, the sintering behavior of an isolated pore of various sizes and shapes at different grain growth rates is studied.

MODEL

The statistical mechanics model that we employ has been successfully applied to study grain boundary wetting. [2] We map a microstructure into a discrete lattice as shown in Fig. 1. A lattice site can be a portion of a grain which is denoted by a letter. Different letters represent different crystalline orientations. A domain of same letters represents a grain. A domain of empty sites represents a pore. There are N possible crystalline orientations. For simplicity, we take the N crystalline orientations to be N planar vectors uniformly spaced on a circle and the angle of a vector is a multiple of $2\pi/N$. The interaction between two vectors depends on the angle difference θ of the two vectors, and in general can be any reasonable function. In the present study, we take

$$V(\theta) = 0 \qquad \text{if } \theta = 0,$$

$$= J \qquad \text{otherwise}. \tag{1}$$

We consider only the nearest-neighbor interactions, i.e., only the interactions between adjacent lattice sites are non-zero. The interaction between a vector and a void (empty site) is J'. The ratio of J'/J determines the T = 0 dihedral angle ψ by $\psi = 2\cos^{-1}(J/2J')$. For example, J'/J = 5/3 gives $\psi = 145°$.

MONTE CARLO KINETICS

Monte Carlo simulations [3] can be a powerful and simple tool for the kinetic study of a

Mat. Res. Soc. Symp. Proc. Vol. 138. ©1989 Materials Research Society

statistical mechanical model when an appropriate kinetic procedure is chosen. In the following, we modify the standard Monte Carlo procedures to allow both grain growth and diffusion during sintering.

Grain Growth

Given a microstructure (with vectors and voids), an occupied site is randomly chosen and randomly assigned a new orientation. The probability that the attempt is successful is

$$W = \frac{1}{\tau_G} e^{-E/kT} \qquad E > 0 \ ,$$

$$= \frac{1}{\tau_G} \qquad E \leq 0 \ ,$$

where E is the energy cost to break all the bonds with its neighbors in order for a vector to flip and $1/\tau_G$ is the attempt frequency associated with orientation flipping.

Diffusion

Diffusion is essential for the densification processes. We model the diffusional process by exchanging the position of a vector with that of its neighboring void. The exchange probability W_{ex} is

$$W_{ex} = \frac{1}{\tau_D} e^{\frac{-\Delta G_{ex}}{kT}} \qquad \Delta G_{ex} > 0$$

$$= \frac{1}{\tau_D} \qquad \Delta G_{ex} \leq 0$$

where ΔG_{ex} is the energy change due to the exchange and $\frac{1}{\tau_D}$ is the attempt frequency for diffusion. The time constant τ_D for diffusion can be in principle different from that for

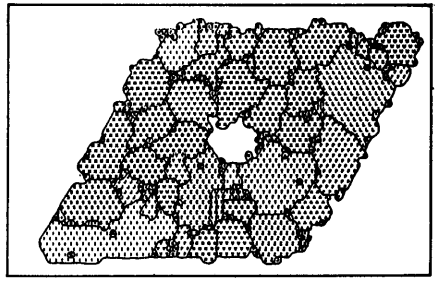

Fig. 1. A lattice representation of a microstructure.

orientation flipping (grain growth) τ_G. We will use the ratio τ_G/τ_D to control the grain growth rate relative to the densification in oversimulation. A large τ_G/τ_D corresponds to slow grain growth.

RESULTS

For all the results shown below, we choose N = 30 and J'/J = 1.67 (equivalent to 145° dihedral angle). Samples were all sintered at $T \sim 0.72\, T_m$ where T_m is the melting temperature. For computational ease, the simulations are all done in two dimensions.

I. General Features of the Model

Figures 2(a)-(d) exhibits the sintering behavior of a multi-pore compact. Figure 2(a) is the initial configuration with 10% porosity. Figure 2(b) is taken at $t = 2000\ \tau_D$. Note that (1) the entire sample is shrinking compared to Figure 2(a), (2) pores are coalescing, and (3) some of the material has evaporated as indicated by the arrow. Figure 2(c) is at $t = 4000\ \tau_D$. Notice that part of the surface has been ruptured as indicated by arrow α. Also notice the rounding of an initially sharp corner as indicated by arrow β. Figure 2(d) is at $t = 50000\ \tau_D$ when the sample is almost fully densified. Note that (1) grains have grown considerably larger, (2) the opening-up of a grain boundary at the surface (thermal etching), and (3) necking has already taken place as indicated by the arrows on the top and at the bottom due to the periodic boundary conditions (initially the upper edge and the lower edge were separated by six layers). The value of τ_G/τ_D is 10 for the above results.

II. Sintering of an Isolated Pore

As an example, we show in Figure 3 the microstructural evolution during the pore sintering of an isolated pore. Figure 3(a) is the initial configuration with a hexagonal pore at the center with edge = 4. Figure 3(b) is at $t = 10000\ \tau_D$. Note the shape of the pore is no longer hexagonal. Figure 3(c) is at $t = 50{,}000\ \tau_D$ when the sample is almost fully densified.

To show the effect of grain growth on the pore shrinkage, in Figure 4 we plot the remaining pore area at $t = 20{,}000\ \tau_D$ for various grain growth rate as a function of the average grain diameter at $t = 20000\ \tau_D$. The arrows indicate the initial pore areas. Each data point is an average of 10 independent runs. The two sets of data correspond to pores with initial area = 61 (edge = 5) and 127 (edge = 7). One can clearly see that the shrinkage of the pores is hindered when grain growth is fast, which is in agreement with the experimental observation of Zhao and Harmer [4]. With further analysis, we find that for a given initial pore size, the pore shrinkage at $t = 20{,}000\ \tau_D$ is proportional to 1/G at $t = 20{,}000\ \tau_D$ where G is the average grain diameter defined as $G \sim \sqrt{A_G}$ where A_G is the average grain area. This behavior may be explained as follows. In the entire process of removing a void from a pore, the bottleneck lies in the break-up of the void from the pore because this process costs most energy. The energy cost of the break-up process can be much reduced when the void is at the interception of the pore surface with a grain boundary. Thus effectively the grain boundaries serve as the channels for transporting the voids. The pore shrinkage rate for large pores is therefore proportional to the number of channels that intercept with the pore surface, which is proportional to 1/G in two dimensions and would be proportional to $1/G^2$ in three dimensions.

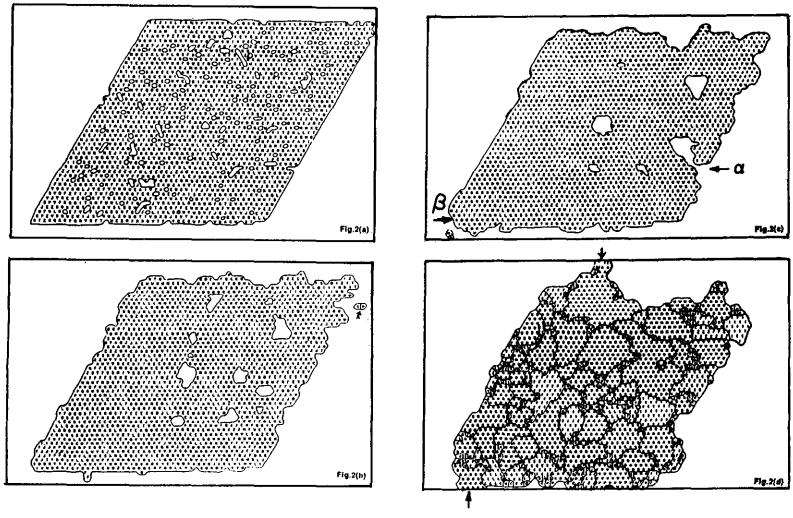

Fig. 2. A typical microstructural evolution of a multi-pore compact, (a) $t=0$, (b) $t=2000\ \tau_D$, (c) $t=4000\ \tau_D$, (d) $t=50000\ \tau_D$.

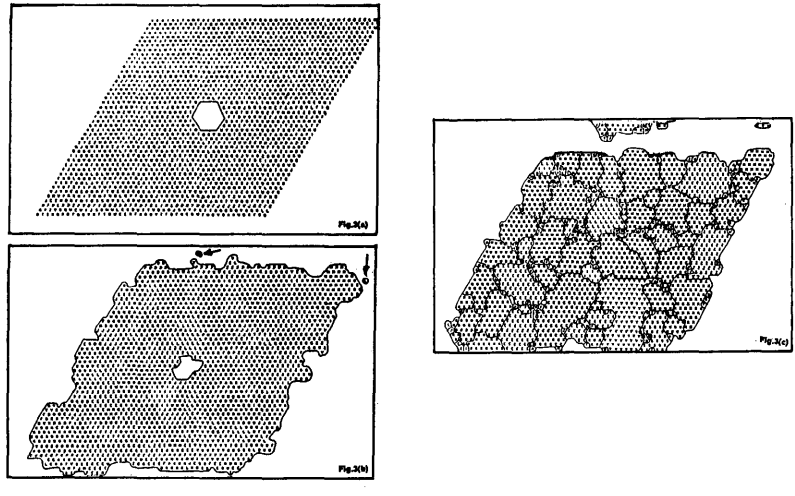

Fig. 3. The microstructural evolution of an isolated hexagonal pore with edge=4, at (a) $t=0$, (b) $t=10000\ \tau_D$, (c) $t=50000\ \tau_D$.

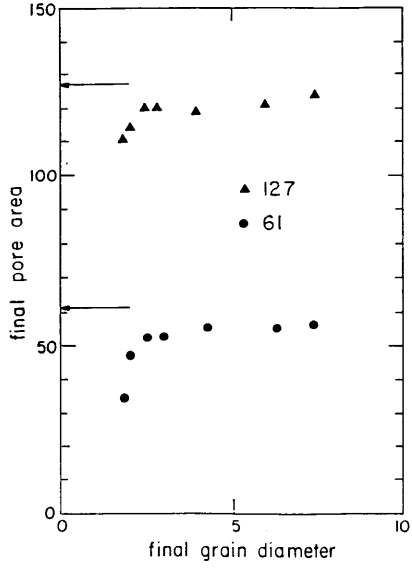

Fig. 4. The average pore area as a function of the average grain diameter at $t = 20000\ \tau_D$.

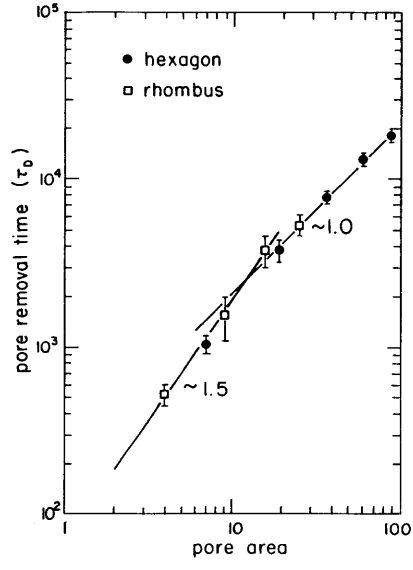

Fig. 5. The pore removal time vs. the initial pore area for fixed sample size of 45x45.

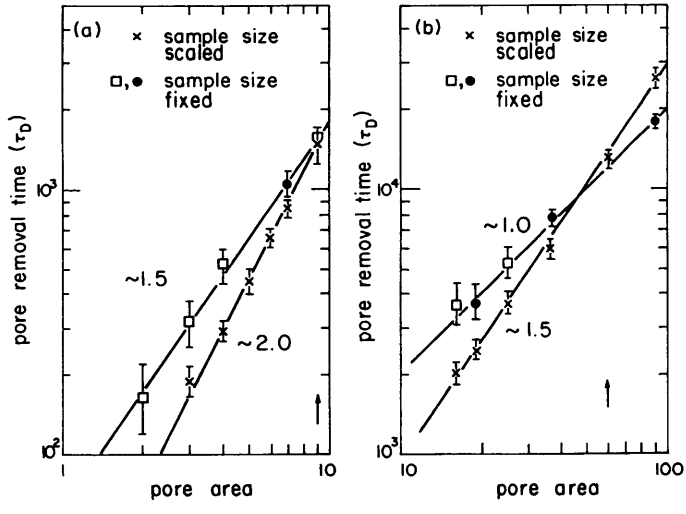

Fig. 6. The pore removal time vs. the initial pore area, (a) for small pores and (b) for large pores. The crosses represent size-scaled samples and the shapes of the pores include triangle, rhombus, and hexagon. The squares and full circles represent the size-fixed samples as shown in Fig. 5.

The effects of the pore size and the pore shape are shown in Figure 5 in which we plot the pore removal time, t_f, as a function of the initial pore area A_p in a double logarithmic scale. In order to separate the effect of grain growth, we do not have orientational flipping in Figure 5, that is, the average grain diameter is fixed at $G \cong 1.8$. Also, the sample size is fixed at 45x45 to separate the effect of different sample sizes. Each data point in Figure 5 is the average of 100 independent runs. It shows that when the pores are large enough, $t_f \sim A_p^{1.0}$, while for small pores, $t_f \sim A_p^{1.5}$. Also note that the pore removal time is initial shape-independent. This is reasonable since the pores are undergoing shape change during sintering as we have shown in Figure 3 and commonly observed experimentally (Ref. 4 is an example).

When properly taking into account the effect of the sample size by changing the sample size proportionally with the pore size, i.e., the pore area to the sample area ratio is fixed as it is in Herring's scaling theory, [5] we obtain $t_f \sim A_p^{2.0}$ for small pores as shown in Figure 6(a) and $t_f \sim A_p^{1.5}$ for large pores as shown in Figure 6(b). In Figure 6, each data point is also the average of 100 independent runs. Also plotted in Figure 6 are the t_f vs. A_p for fixed sample size for comparison. From Figure 6, it is clear that the change of sample size gives the additional $A_p^{0.5}$ dependence. The fact that $t_f \sim A_p^{2.0}$ for small pores and $t_f \sim A_p^{1.5}$ for large pores for size-scaled samples indicates that for small pores, surface diffusion is the dominant mechanism (r_p^4 dependence) and for large pores, volume diffusion (r_p^3 dependence) [5] is the dominant mechanism where $r_p \sim \sqrt{A_p}$ is the average pore diameter. The crossover from small pore behavior (r_p^4) to large pore behavior (r_p^3) occurs when the pore size r_p becomes larger than the grain size G.

CONCLUSIONS

We have constructed a statistical mechanics sintering model for the first time. The model is capable of displaying various sintering phenomena such as evaporation and condensation, rounding of a sharp corner, pore coalescence, thermal etching, neck-formation, grain growth, etc. For an isolated pore, we showed that grain growth can slow down the pore shrinkage. Furthermore, the pore removal time t_f is independent of the initial pore shape and, for fixed sample size, $t_f \sim A_p^{1.5}$ for small pores and $t_f \sim A_p^{1.0}$ for large pores. After scaling up the sample size with the pore size, $t_f \sim A_p^{2.0}$ for small pores and $t_f \sim A_p^{1.5}$ for large pores, which is in good agreement with Herring's scaling theory. Our results indicate that the dominant mass transport mechanism is surface diffusion for small pores and volume diffusion for large pores. The crossover occurs when the pore size is comparable with the grain size.

ACKNOWLEDGMENTS

This work is supported by AFOSR and DARPA under Grant No. AFOSR-87-0114.

REFERENCES

1. M. P. Anderson, D. J. Srolovitz, G. S. Grest, and P. S. Sahni, *Acta Metall.* **32**, 783 (1984).
2. M. Schick and W.-H. Shih, *Phys. Rev. B* **35**, 5030 (1987).
3. K. Binder, ed., ***Application of the Monte Carlo Method in Statistical Physics***, Springer-Verlag, 1987.
4. J. Zhao and M. P. Harmer, *J. Amer. Ceram. Soc.* **71**, 530 (1988).
5. C. Herring, *J. Appl. Phys.* **21**, 301 (1950).